Table of Contents

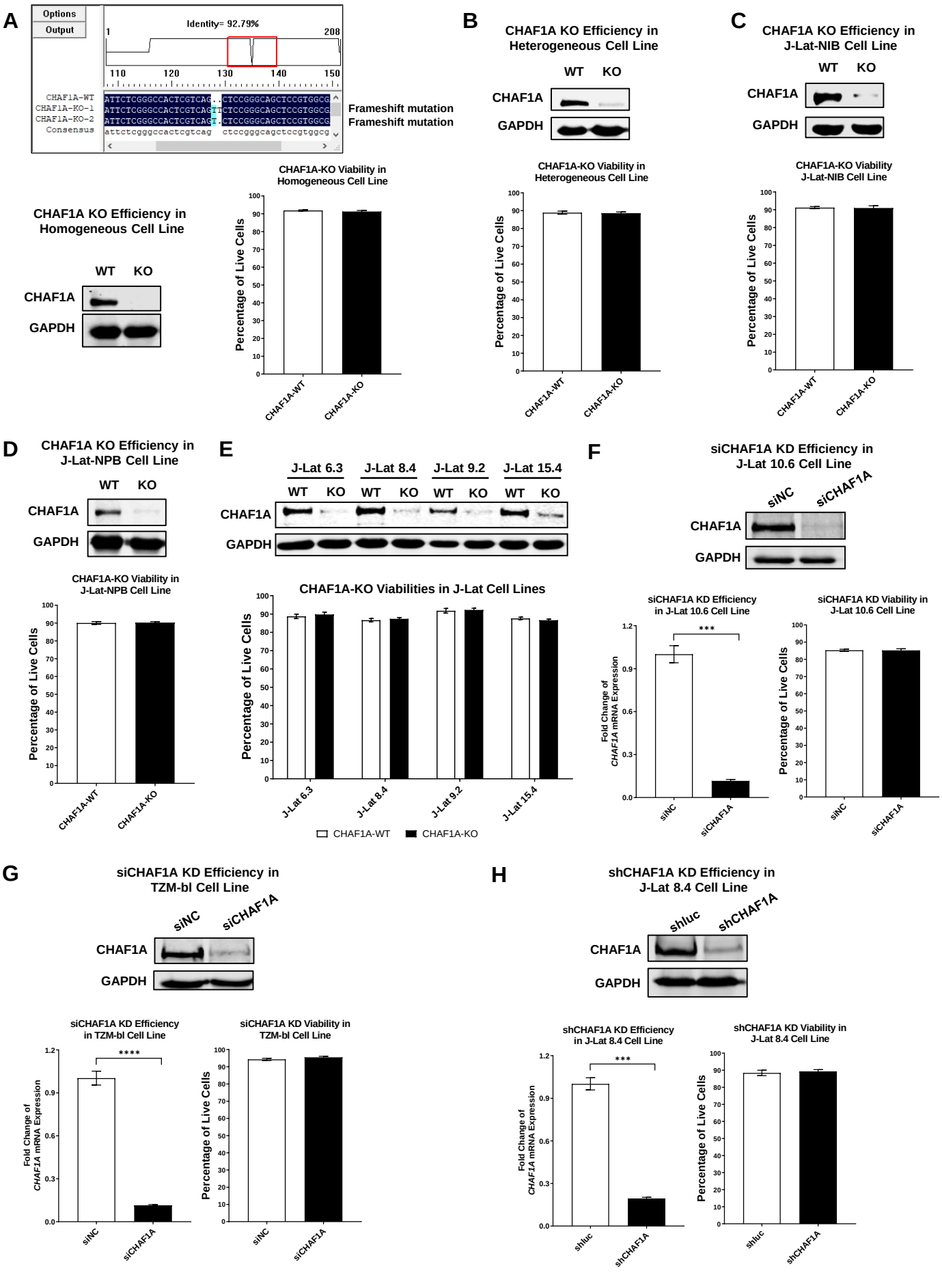
A
Options
Output
Identity= 92.79%
1
208
110
120
130
140
150
CHAF1A-WT
CHAF1A-KO-1
CHAF1A-KO-2
Consensus
Frameshift mutation
Frameshift mutation
CHAF1A KO Efficiency in Homogeneous Cell Line
WT
KO
CHAF1A
GAPDH
CHAF1A-KO Viability in Homogeneous Cell Line
Percentage of Live Cells
CHAF1A-WT
CHAF1A-KO
B
CHAF1A KO Efficiency in Heterogeneous Cell Line
WT
KO
CHAF1A
GAPDH
CHAF1A-KO Viability in Heterogeneous Cell Line
Percentage of Live Cells
CHAF1A-WT
CHAF1A-KO
C
CHAF1A KO Efficiency in J-Lat-NIB Cell Line
WT
KO
CHAF1A
GAPDH
CHAF1A-KO Viability J-Lat-NIB Cell Line
Percentage of Live Cells
CHAF1A-WT
CHAF1A-KO
D
CHAF1A KO Efficiency in J-Lat-NPB Cell Line
WT
KO
CHAF1A
GAPDH
CHAF1A-KO Viability in J-Lat-NPB Cell Line
Percentage of Live Cells
CHAF1A-WT
CHAF1A-KO
E
J-Lat 6.3
J-Lat 8.4
J-Lat 9.2
J-Lat 15.4
WT
KO
CHAF1A
GAPDH
CHAF1A-KO Viabilities in J-Lat Cell Lines
Percentage of Live Cells
J-Lat 6.3
J-Lat 8.4
J-Lat 9.2
J-Lat 15.4
CHAF1A-WT
CHAF1A-KO
F
siCHAF1A KD Efficiency in J-Lat 10.6 Cell Line
siNC
siCHAF1A
CHAF1A
GAPDH
siCHAF1A KD Efficiency in J-Lat 10.6 Cell Line
***
Fold Change of CHAF1A mRNA Expression
siNC
siCHAF1A
siCHAF1A KD Viability in J-Lat 10.6 Cell Line
Percentage of Live Cells
siNC
siCHAF1A
G
siCHAF1A KD Efficiency in TZM-bl Cell Line
siNC
siCHAF1A
CHAF1A
GAPDH
siCHAF1A KD Efficiency in TZM-bl Cell Line
****
Fold Change of CHAF1A mRNA Expression
siNC
siCHAF1A
siCHAF1A KD Viability in TZM-bl Cell Line
Percentage of Live Cells
siNC
siCHAF1A
H
shCHAF1A KD Efficiency in J-Lat 8.4 Cell Line
shluc
shCHAF1A
CHAF1A
GAPDH
shCHAF1A KD Efficiency in J-Lat 8.4 Cell Line
***
Fold Change of CHAF1A mRNA Expression
shluc
shCHAF1A
shCHAF1A KD Viability in J-Lat 8.4 Cell Line
Percentage of Live Cells
shluc
shCHAF1A

Appendix Figure S1. Knockdown or knockout efficiencies and corresponding viabilities data.

A Sequencing results of J-Lat 10.6 CHAF1A-KO homogeneous cell line (named P1D9). Both alleles of *CHAF1A* gene were frameshift mutated. The lower left panel indicated the knockout efficiency which was confirmed by WB. The lower right panel indicated the percentages of viable cells which were quantitated by measuring the percentages of amine-reactive fluorescent dye non-permeant cells.

B-E The knockout efficiencies in heterogeneous J-Lat 10.6 cell line, J-Lat-NIB cell line, J-Lat-NPB cell line as well as six monoclonal J-Lat cell lines (J-lat 6.3, 8.4, 9.2 and 15.4) were confirmed by WB. The corresponding viabilities upon CHAF1A knockout in each cell line were quantitated by measuring the percentages of amine-reactive fluorescent dye non-permeant cells.

F-H The efficiencies of siCHAF1A-mediated CHAF1A knockdown in J-Lat 10.6, siCHAF1A-mediated CHAF1A knockdown in TZM-bl and shCHAF1A-mediated CHAF1A knockdown in J-Lat 8.4 were confirmed by both WB and qPCR. The viabilities upon CHAF1A knockdown in each cell line were quantitated as in (A).

Data information: Data represented mean ± SEM in triplicate. p-Values were calculated by Student's *t*-test. ***$p < 0.001$, **** $p < 0.0001$.

Source data are available online for this figure.

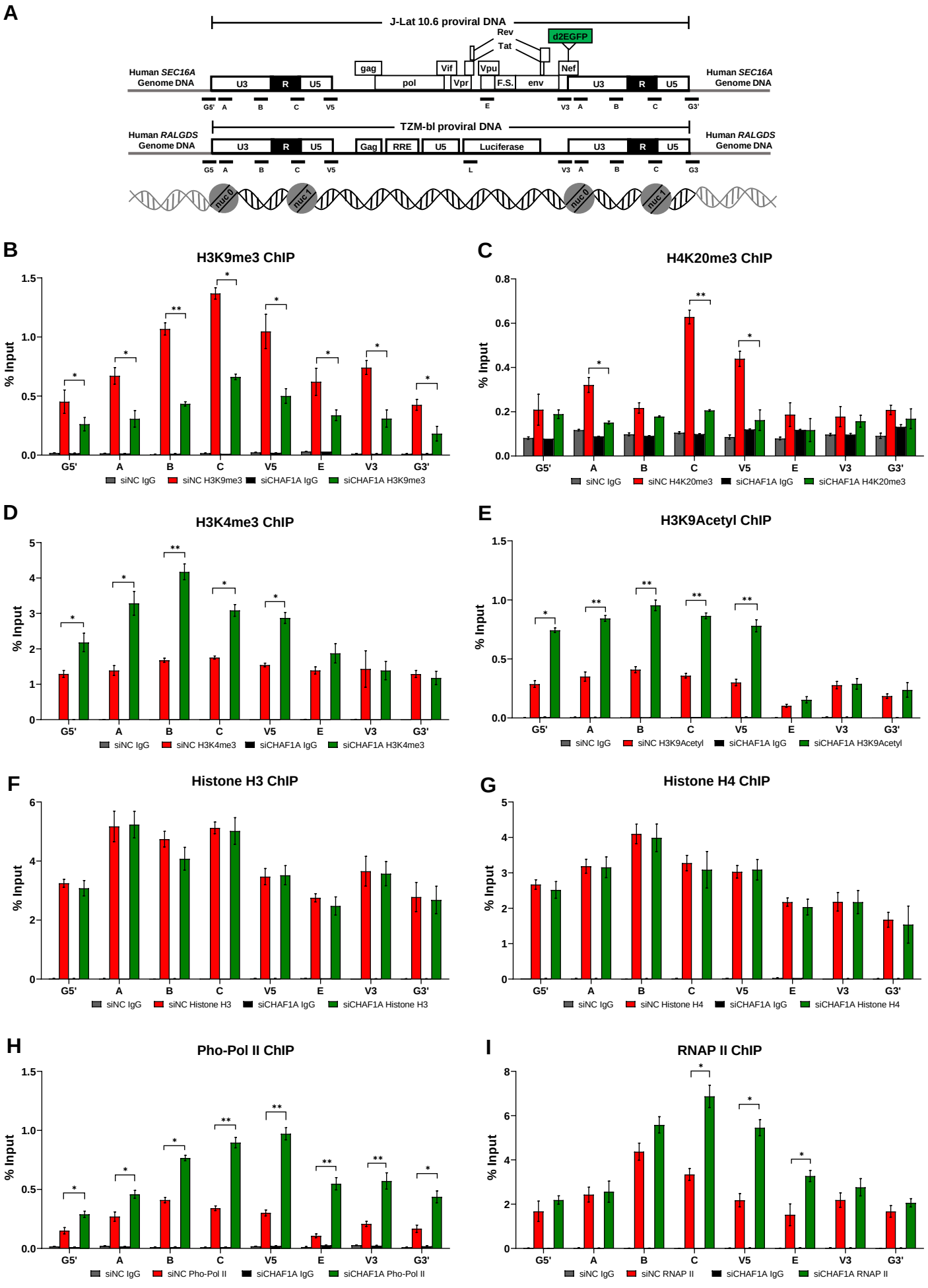
A
J-Lat 10.6 proviral DNA
Rev
Tat
d2EGFP
Human SEC16A Genome DNA
gag
Vif
Vpu
Nef
pol
Vpr
F.S.
env
U3
R
U5
G5'
A
B
C
V5
E
V3
G3'
TZM-bl proviral DNA
Human RALGDS Genome DNA
Gag
RRE
Luciferase
G5
L
nuc 0
nuc 1
B
H3K9me3 ChIP
% Input
siNC IgG
siNC H3K9me3
siCHAF1A IgG
siCHAF1A H3K9me3
C
H4K20me3 ChIP
siNC H4K20me3
siCHAF1A H4K20me3
D
H3K4me3 ChIP
siNC H3K4me3
siCHAF1A H3K4me3
E
H3K9Acetyl ChIP
siNC H3K9Acetyl
siCHAF1A H3K9Acetyl
F
Histone H3 ChIP
siNC Histone H3
siCHAF1A Histone H3
G
Histone H4 ChIP
siNC Histone H4
siCHAF1A Histone H4
H
Pho-Pol II ChIP
siNC Pho-Pol II
siCHAF1A Pho-Pol II
I
RNAP II ChIP
siNC RNAP II
siCHAF1A RNAP II

Appendix Figure S2. ChIP-qPCR of different targets on HIV-1 LTR upon CHAF1A knockdown.

A Schematic of HIV-1 proviruses within J-Lat 10.6 and TZM-bl. HIV-1 genomic DNA was integrated in the intron of cellular gene *SEC16A* in J-Lat 10.6. HIV-1 mini-genomic DNA was integrated in the intron of cellular gene *RALGDS* in TZM-bl. The ChIP-qPCR primers were indicated below each backbone. G5' represented cellular DNA and viral 5'LTR junction in J-Lat 10.6; A: Nucleosome 0 assembly site; B: Nucleosome free region; C: Nucleosome 1 assembly site; V5: Viral 5'LTR and gag leader sequence junction; E represented *envelope*; V3: Viral poly purine tract and 3'LTR junction; G3' represented viral 3'LTR and cellular DNA junction; G5 represented cellular DNA and viral 5'LTR junction in TZM-bl; L represented *luciferase* gene region; G3 represented viral 3'LTR and cellular DNA junction in TZM-bl.

B-I ChIP assays with antibodies against H3K9me3, H4K20me3, H3K4me3, H3K9Acetyl, Histone H3, Histone H4, Pho-Pol II and RNAP II were performed in siNC and siCHAF1A J-Lat 10.6 cells. ChIP signals along the viral genome (represented by 8 positions) within each group were normalized to Input.

Data information: Data represented mean ± SEM in triplicate. p-Values were calculated by Student's *t*-test. *$p < 0.05$, **$p < 0.01$.

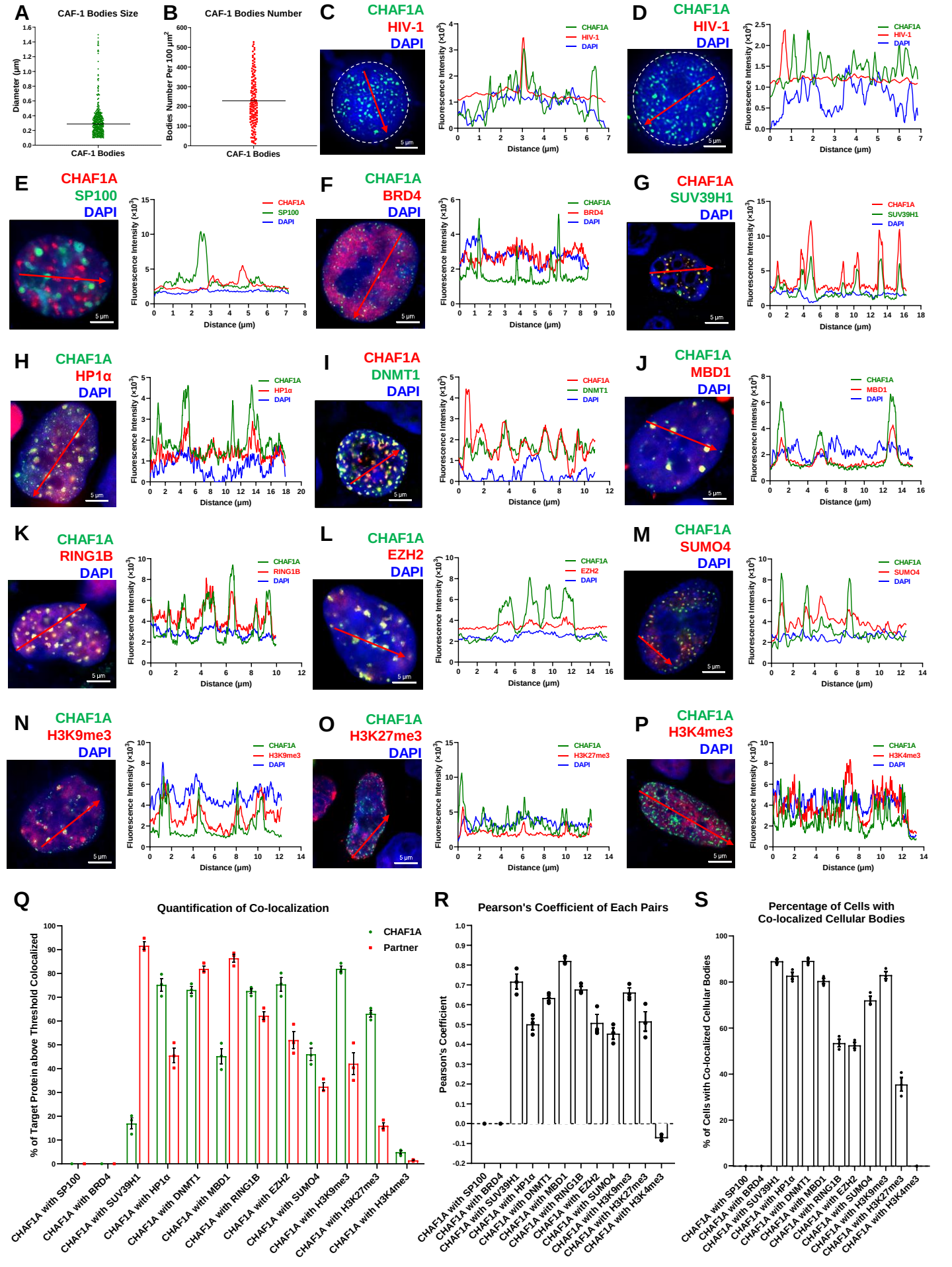
A
CAF-1 Bodies Size
Diameter (μm)
CAF-1 Bodies
B
CAF-1 Bodies Number
Bodies Number Per 100 μm²
CAF-1 Bodies
C
CHAF1A
HIV-1
DAPI
D
CHAF1A
HIV-1
DAPI
E
CHAF1A
SP100
DAPI
F
CHAF1A
BRD4
DAPI
G
CHAF1A
SUV39H1
DAPI
H
CHAF1A
HP1α
DAPI
I
CHAF1A
DNMT1
DAPI
J
CHAF1A
MBD1
DAPI
K
CHAF1A
RING1B
DAPI
L
CHAF1A
EZH2
DAPI
M
CHAF1A
SUMO4
DAPI
N
CHAF1A
H3K9me3
DAPI
O
CHAF1A
H3K27me3
DAPI
P
CHAF1A
H3K4me3
DAPI
Fluorescence Intensity (×10³)
Distance (μm)
5 μm
Q
Quantification of Co-localization
% of Target Protein above Threshold Colocalized
CHAF1A
Partner
CHAF1A with SP100
CHAF1A with BRD4
CHAF1A with SUV39H1
CHAF1A with HP1α
CHAF1A with DNMT1
CHAF1A with MBD1
CHAF1A with RING1B
CHAF1A with EZH2
CHAF1A with SUMO4
CHAF1A with H3K9me3
CHAF1A with H3K27me3
CHAF1A with H3K4me3
R
Pearson's Coefficient of Each Pairs
Pearson's Coefficient
S
Percentage of Cells with Co-localized Cellular Bodies
% of Cells with Co-localized Cellular Bodies

Appendix Figure S3. Co-localization analysis of CAF-1 body components.

A The distribution of CAF-1 bodies diameters. Data were collected from 30 cells of 10 samples which were prepared in 10 independent experiments.

B The distribution of CAF-1 bodies numbers per 100 μm^2. Data were collected from 143 distinct nuclei sections from 50 cells of 10 samples which were prepared in 10 independent experiments.

C, D The line scan profiles of ImmunoFISH images which showed the positions of CHAF1A bodies and HIV-1 DNA in both naïve and activated statuses. The red arrows indicated the positions where the line scans showed.

E-P The line scan profiles of SIM images which showed co-localization and non-co-localization between CHAF1A and its partners.

Q Quantification analysis of co-localization of CHAF1A and its partners. Total volumes of CHAF1A and its partners as well as co-localized parts were measured. Percentages of CHAF1A above threshold co-localized were calculated by measuring the percentages of co-localized CHAF1A volume in total CHAF1A volume. Percentages of CHAF1A partners above threshold co-localized were calculated by measuring the percentages of co-localized target protein volume in total target protein volume.

R Pearson's coefficients in co-localized volume of each protein pairs were calculated based on the quantitation analysis results showed in (Q). The co-localization value ranges between 1 and -1. A value of 1 represents perfect co-localization, 0 represents no co-localization, and -1 represents perfect inverse correlation.

S The percentages of cells with co-localized cellular bodies.

Data information: The scale bar of each SIM image represented 5 μm. All the samples were imaged to obtain at least three images. All the merged SIM images used for line scan profiling in (C-P) were from Fig 3C to Fig 3P.

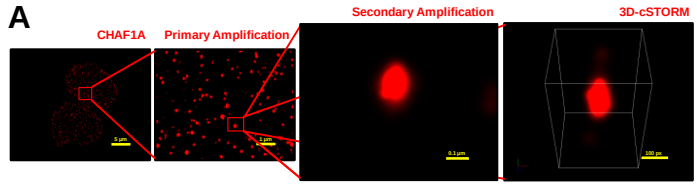
A
CHAF1A
Primary Amplification
Secondary Amplification
3D-cSTORM

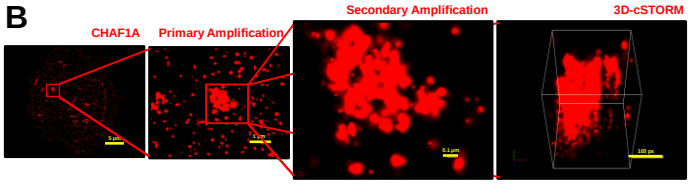
B
CHAF1A
Primary Amplification
Secondary Amplification
3D-cSTORM

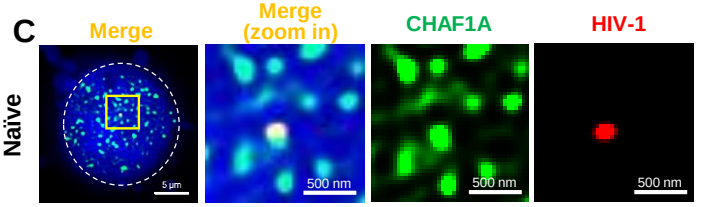
C
Naïve
Merge
Merge (zoom in)
CHAF1A
HIV-1
500 nm

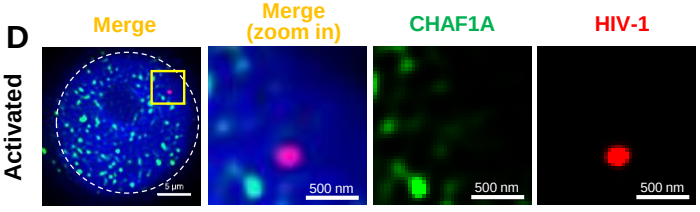
D
Activated
Merge
Merge (zoom in)
CHAF1A
HIV-1
500 nm

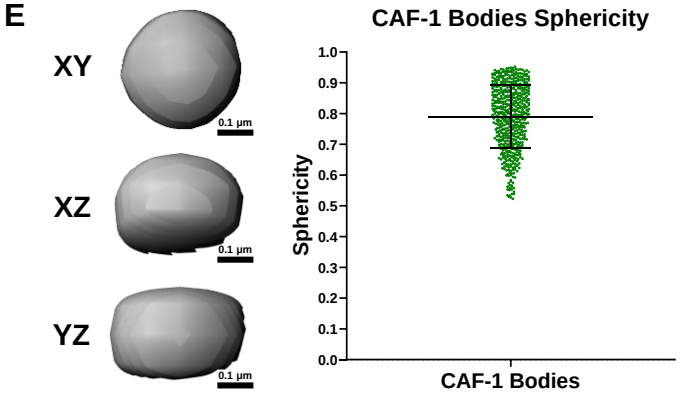
E
XY
XZ
YZ
0.1 μm
CAF-1 Bodies Sphericity
Sphericity
CAF-1 Bodies

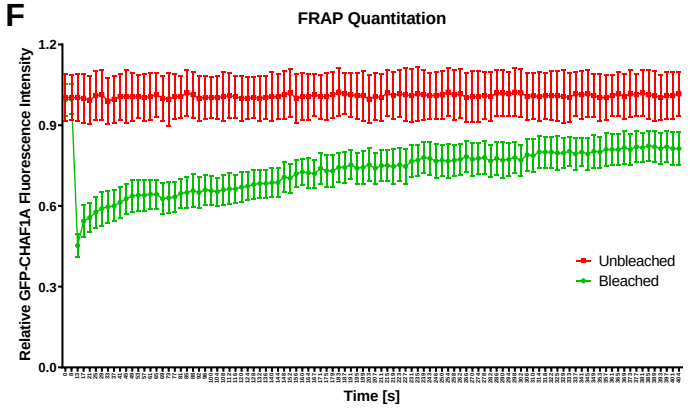
F
FRAP Quantitation
Relative GFP-CHAF1A Fluorescence Intensity
Time [s]
Unbleached
Bleached

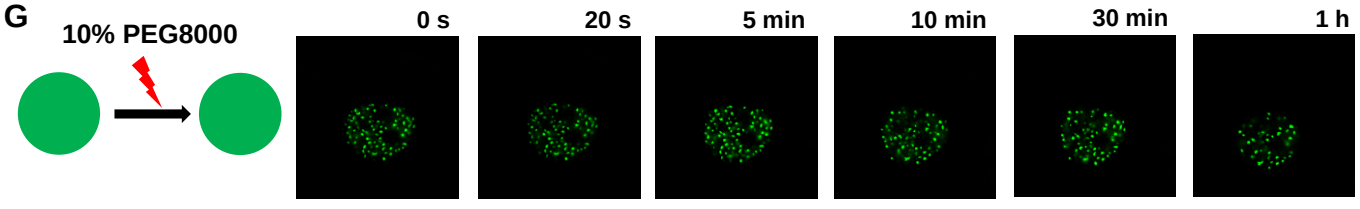
G
10% PEG8000
0 s
20 s
5 min
10 min
30 min
1 h

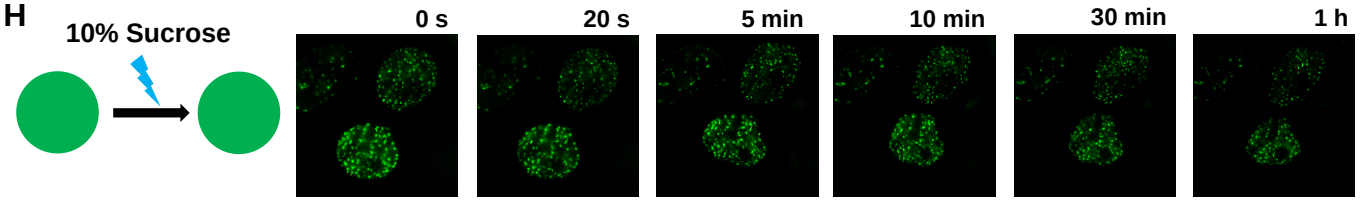
H
10% Sucrose
0 s
20 s
5 min
10 min
30 min
1 h

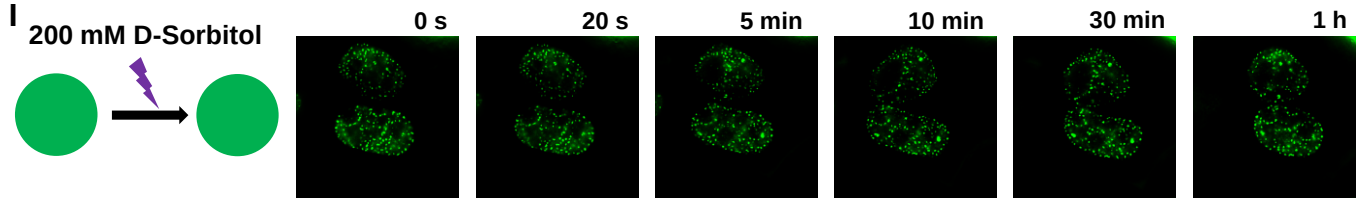
I
200 mM D-Sorbitol
0 s
20 s
5 min
10 min
30 min
1 h

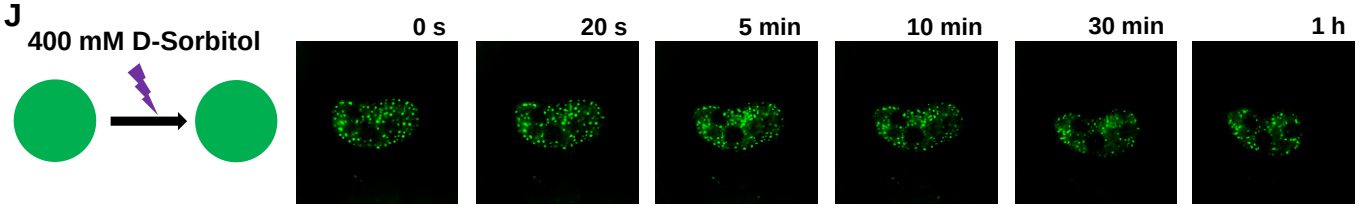
J
400 mM D-Sorbitol
0 s
20 s
5 min
10 min
30 min
1 h

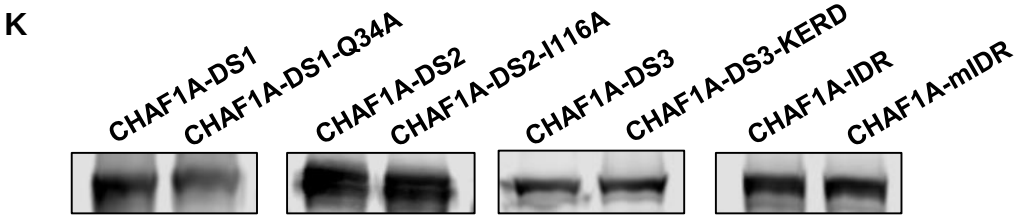
K
CHAF1A-DS1
CHAF1A-DS1-Q34A
CHAF1A-DS2
CHAF1A-DS2-I116A
CHAF1A-DS3
CHAF1A-DS3-KERD
CHAF1A-IDR
CHAF1A-mIDR

Appendix Figure S4. The LLPS properties of CAF-1 bodies.

A, B Super-resolution cSTORM images of CAF-1 bodies. Isolated and clustered CAF-1 bodies were amplified and displayed in 2D and 3D. Two degrees of amplification were performed for CAF-1 bodies.

C, D Amplified ImmunoFISH images of CAF-1 bodies and HIV-1 genomic DNA within J-Lat 10.6. Images showed both naïve and TNFα-activated J-Lat 10.6 cells.

E Rendered 3D shapes of CAF-1 bodies. Three panels indicated XY, XZ and YZ planes of the CAF-1 body. The right scatter plot represented the distribution of CAF-1 bodies sphericities. Data were collected from 579 CAF-1 bodies of five cells from five samples which were prepared in five independent experiments.

F FRAP histogram of unbleached and bleached CAF-1 bodies. Six unbleached and six bleached CAF-1 bodies from six different cells were observed to record fluorescence intensities for 404 seconds (over 6 minutes).

G-J GFP-CHAF1A-expressing HEK293T cells were treated with 10% PEG8000, 10% Sucrose, 200 mM D-Sorbitol and 400 mM D-Sorbitol respectively. Live cells images of pre-treatment, as well as 20 s, 5 min, 10 min, 30 min and 1 h post-treatment were captured.

K The expression of *in vitro* purified CHAF1A-DS1, CHAF1A-DS2, CHAF1A-DS3, CHAF1A-IDR and corresponding mutants was confirmed by WB.

Data information: The scale bar of each SIM image represented 5 μm. The scale bars of amplified STORM images in (A) and (B) represented 1 μm (primary amplification) and 0.1 μm (secondary amplification). The scale bar of 3D-cSTORM represented 100 px. The scale bar of each amplified image in (C) and (D) represented 500 nm. All the samples were imaged to obtain at least three images.

Source data are available online for this figure.

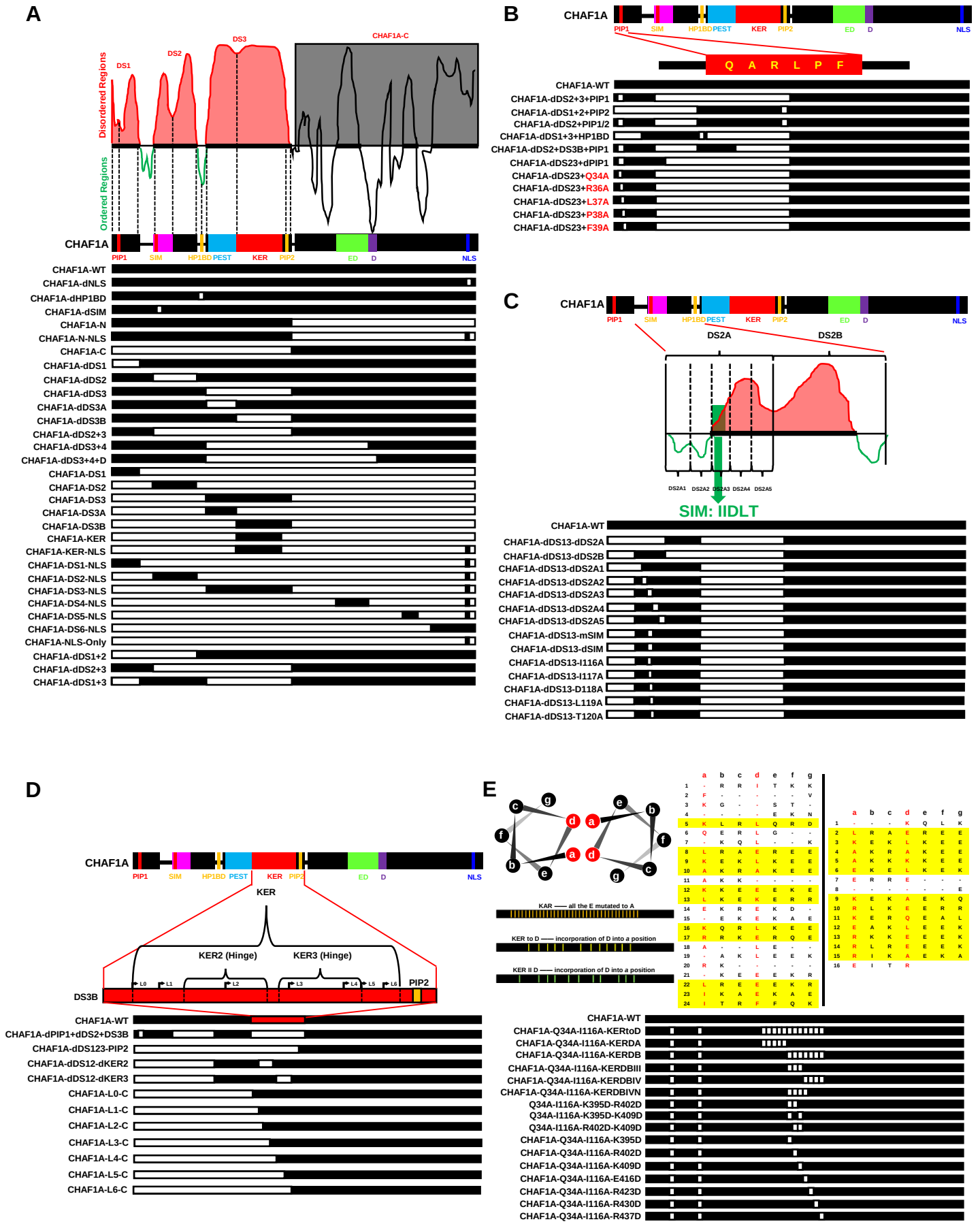
A
Disordered Regions
Ordered Regions
DS1
DS2
DS3
CHAF1A-C
CHAF1A
PIP1
SIM
HP1BD
PEST
KER
PIP2
ED
D
NLS
CHAF1A-WT
CHAF1A-dNLS
CHAF1A-dHP1BD
CHAF1A-dSIM
CHAF1A-N
CHAF1A-N-NLS
CHAF1A-C
CHAF1A-dDS1
CHAF1A-dDS2
CHAF1A-dDS3
CHAF1A-dDS3A
CHAF1A-dDS3B
CHAF1A-dDS2+3
CHAF1A-dDS3+4
CHAF1A-dDS3+4+D
CHAF1A-DS1
CHAF1A-DS2
CHAF1A-DS3
CHAF1A-DS3A
CHAF1A-DS3B
CHAF1A-KER
CHAF1A-KER-NLS
CHAF1A-DS1-NLS
CHAF1A-DS2-NLS
CHAF1A-DS3-NLS
CHAF1A-DS4-NLS
CHAF1A-DS5-NLS
CHAF1A-DS6-NLS
CHAF1A-NLS-Only
CHAF1A-dDS1+2
CHAF1A-dDS2+3
CHAF1A-dDS1+3
B
CHAF1A
PIP1
SIM
HP1BD
PEST
KER
PIP2
ED
D
NLS
Q A R L P F
CHAF1A-WT
CHAF1A-dDS2+3+PIP1
CHAF1A-dDS1+2+PIP2
CHAF1A-dDS2+PIP1/2
CHAF1A-dDS1+3+HP1BD
CHAF1A-dDS2+DS3B+PIP1
CHAF1A-dDS23+dPIP1
CHAF1A-dDS23+Q34A
CHAF1A-dDS23+R36A
CHAF1A-dDS23+L37A
CHAF1A-dDS23+P38A
CHAF1A-dDS23+F39A
C
CHAF1A
PIP1
SIM
HP1BD
PEST
KER
PIP2
ED
D
NLS
DS2A
DS2B
DS2A1
DS2A2
DS2A3
DS2A4
DS2A5
SIM: IIDLT
CHAF1A-WT
CHAF1A-dDS13-dDS2A
CHAF1A-dDS13-dDS2B
CHAF1A-dDS13-dDS2A1
CHAF1A-dDS13-dDS2A2
CHAF1A-dDS13-dDS2A3
CHAF1A-dDS13-dDS2A4
CHAF1A-dDS13-dDS2A5
CHAF1A-dDS13-mSIM
CHAF1A-dDS13-dSIM
CHAF1A-dDS13-I116A
CHAF1A-dDS13-I117A
CHAF1A-dDS13-D118A
CHAF1A-dDS13-L119A
CHAF1A-dDS13-T120A
D
CHAF1A
PIP1
SIM
HP1BD
PEST
KER
PIP2
ED
D
NLS
KER
KER2 (Hinge)
KER3 (Hinge)
L0
L1
L2
L3
L4
L5
L6
DS3B
PIP2
CHAF1A-WT
CHAF1A-dPIP1+dDS2+DS3B
CHAF1A-dDS123-PIP2
CHAF1A-dDS12-dKER2
CHAF1A-dDS12-dKER3
CHAF1A-L0-C
CHAF1A-L1-C
CHAF1A-L2-C
CHAF1A-L3-C
CHAF1A-L4-C
CHAF1A-L5-C
CHAF1A-L6-C
E
KAR —— all the E mutated to A
KER to D —— incorporation of D into a position
KER II D —— incorporation of D into a position
CHAF1A-WT
CHAF1A-Q34A-I116A-KERtoD
CHAF1A-Q34A-I116A-KERDA
CHAF1A-Q34A-I116A-KERDB
CHAF1A-Q34A-I116A-KERDBIII
CHAF1A-Q34A-I116A-KERDBIV
CHAF1A-Q34A-I116A-KERDBIVN
Q34A-I116A-K395D-R402D
Q34A-I116A-K395D-K409D
Q34A-I116A-R402D-K409D
CHAF1A-Q34A-I116A-K395D
CHAF1A-Q34A-I116A-R402D
CHAF1A-Q34A-I116A-K409D
CHAF1A-Q34A-I116A-E416D
CHAF1A-Q34A-I116A-R423D
CHAF1A-Q34A-I116A-R430D
CHAF1A-Q34A-I116A-R437D

Appendix Figure S5. The procedure to identify the key amino acids which mediated the LLPS of CAF-1 body.

A Upper panel showed the schematic of CHAF1A disordered regions. Specific segments including PIP1, SIM, HP1BD, PEST, KER, PIP2, ED, D and NLS were labelled below. Lower panels of CHAF1A mutants were used to identify the IDRs which mediated the LLPS of CHAF1A.

B CHAF1A mutants that were used to identify the key amino acids which mediated the LLPS of DS1.

C CHAF1A mutants that were used to identify the key amino acids which mediated the LLPS of DS2.

D Segmentation strategy that was used to identify the shortest segment which mediated the LLPS of DS3.

E Upper panels showed the prediction results of KER coiled-coil structure and corresponding three CHAF1A mutants. The amino acids within coiled-coil interface were mutated to aspartic acid (Asp or D). The low panels of CHAF1A mutants were used to identify the minimum numbers of amino acid mutation which mediated the LLPS of DS3 and CHAF1A.

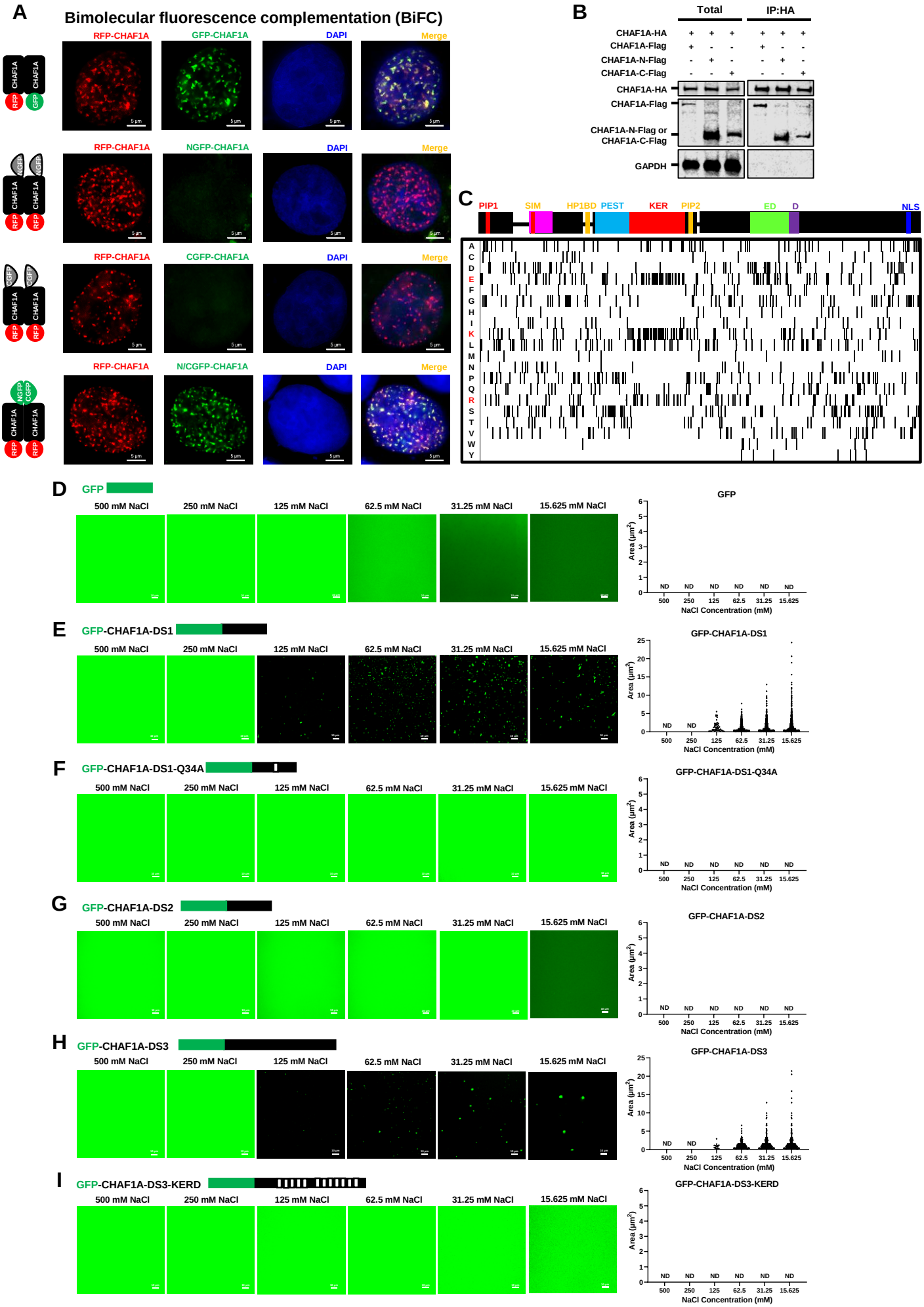
A
Bimolecular fluorescence complementation (BiFC)
RFP-CHAF1A
GFP-CHAF1A
DAPI
Merge
NGFP-CHAF1A
CGFP-CHAF1A
N/CGFP-CHAF1A
B
Total
IP:HA
CHAF1A-HA
CHAF1A-Flag
CHAF1A-N-Flag
CHAF1A-C-Flag
CHAF1A-N-Flag or
CHAF1A-C-Flag
GAPDH
C
PIP1
SIM
HP1BD
PEST
KER
PIP2
ED
D
NLS
D
GFP
E
GFP-CHAF1A-DS1
F
GFP-CHAF1A-DS1-Q34A
G
GFP-CHAF1A-DS2
H
GFP-CHAF1A-DS3
I
GFP-CHAF1A-DS3-KERD
500 mM NaCl
250 mM NaCl
125 mM NaCl
62.5 mM NaCl
31.25 mM NaCl
15.625 mM NaCl
Area (μm²)
NaCl Concentration (mM)
ND

Appendix Figure S6. Three IDRs mediate the LLPS of CAF-1 body.

A Bimolecular fluorescence complementation (BiFC) experiment of CHAF1A. GFP sequence was divided into NGFP and CGFP which were conjugated to CHAF1A sequence. GFP-tagged CHAF1A, NGFP-tagged CHAF1A and CGFP-tagged CHAF1A were co-overexpressed with RFP-tagged CHAF1A respectively. The lower panel indicated that RFP-tagged, NGFP-tagged and CGFP-tagged CHAF1A were transfected simultaneously.

B Flag-tagged CHAF1A, Flag-tagged CHAF1A-N and Flag-tagged CHAF1A-C were co-overexpressed with HA-tagged CHAF1A. Cell lysates of each group were IP with anti-HA beads and IB with anti-HA, anti-Flag and anti-GAPDH antibodies. Both total and IP samples were developed.

C Composition analysis of CHAF1A protein. Lower table indicated the distribution of twenty kinds of amino acids.

D-I GFP, GFP-CHAF1A-DS1, GFP-CHAF1A-DS1-Q34A, GFP-CHAF1A-DS2, GFP-CHAF1A-DS3 and GFP-CHAF1A-DS3-KERD were expressed and purified *in vitro*. Ten micromole of each protein was proceeded to the droplet formation buffer which contained six concentration gradients of NaCl. Statistical analysis results of body areas and numbers were shown aside.

Data information: The scale bars in (A) represented 5 μm. The scale bars in (D-I) represented 10 μm.

Source data are available online for this figure.

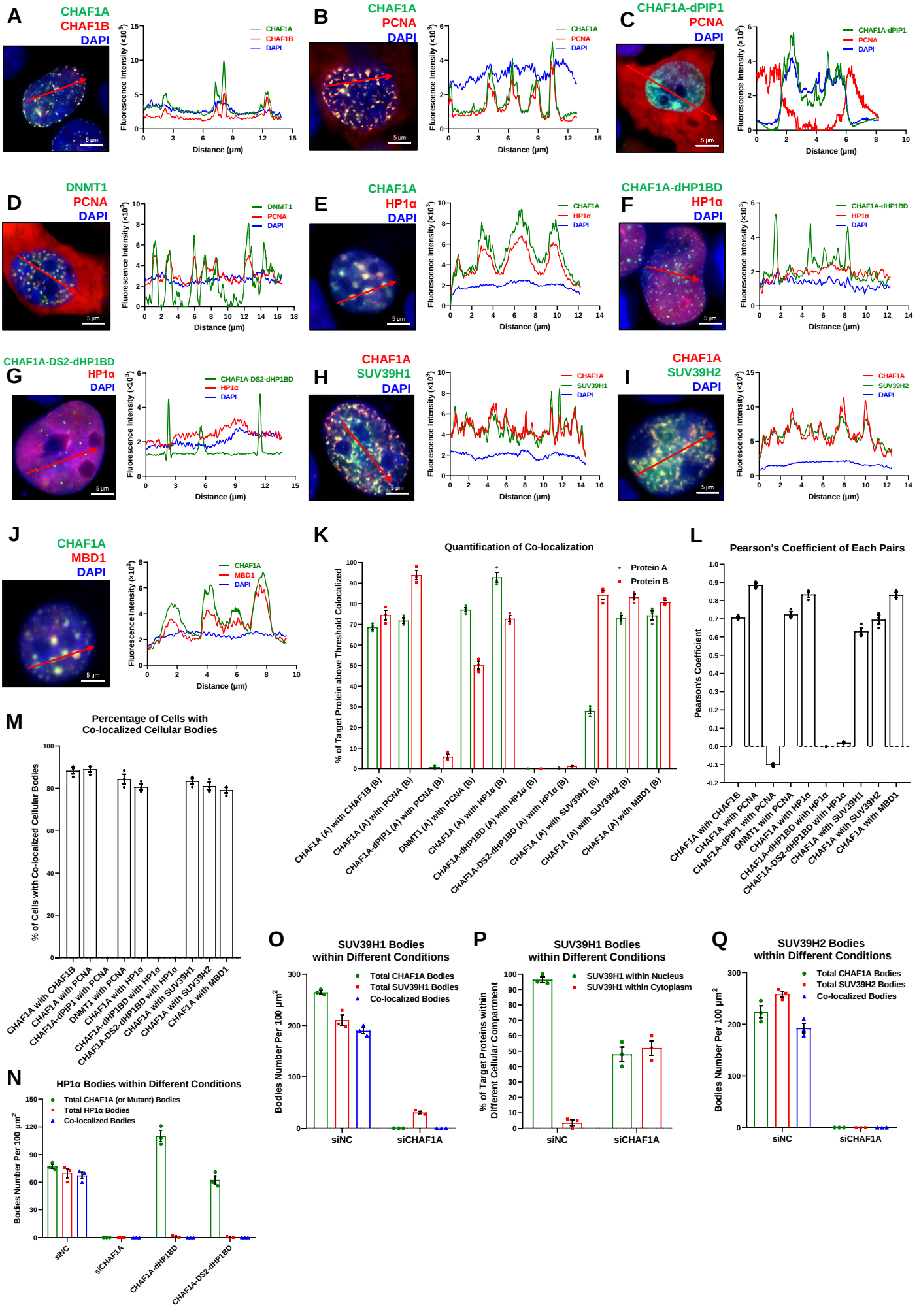
A
CHAF1A
CHAF1B
DAPI
Fluorescence Intensity (×10³)
Distance (μm)
B
CHAF1A
PCNA
DAPI
C
CHAF1A-dPIP1
PCNA
DAPI
D
DNMT1
PCNA
DAPI
E
CHAF1A
HP1α
DAPI
F
CHAF1A-dHP1BD
HP1α
DAPI
G
CHAF1A-DS2-dHP1BD
HP1α
DAPI
H
CHAF1A
SUV39H1
DAPI
I
CHAF1A
SUV39H2
DAPI
J
CHAF1A
MBD1
DAPI
K
Quantification of Co-localization
% of Target Protein above Threshold Colocalized
Protein A
Protein B
CHAF1A (A) with CHAF1B (B)
CHAF1A (A) with PCNA (B)
CHAF1A-dPIP1 (A) with PCNA (B)
DNMT1 (A) with PCNA (B)
CHAF1A (A) with HP1α (B)
CHAF1A-dHP1BD (A) with HP1α (B)
CHAF1A-DS2-dHP1BD (A) with HP1α (B)
CHAF1A (A) with SUV39H1 (B)
CHAF1A (A) with SUV39H2 (B)
CHAF1A (A) with MBD1 (B)
L
Pearson's Coefficient of Each Pairs
Pearson's Coefficient
CHAF1A with CHAF1B
CHAF1A with PCNA
CHAF1A-dPIP1 with PCNA
DNMT1 with PCNA
CHAF1A with HP1α
CHAF1A-dHP1BD with HP1α
CHAF1A-DS2-dHP1BD with HP1α
CHAF1A with SUV39H1
CHAF1A with SUV39H2
CHAF1A with MBD1
M
Percentage of Cells with
Co-localized Cellular Bodies
% of Cells with Co-localized Cellular Bodies
CHAF1A with CHAF1B
CHAF1A with PCNA
CHAF1A-dPIP1 with PCNA
DNMT1 with PCNA
CHAF1A with HP1α
CHAF1A-dHP1BD with HP1α
CHAF1A-DS2-dHP1BD with HP1α
CHAF1A with SUV39H1
CHAF1A with SUV39H2
CHAF1A with MBD1
N
HP1α Bodies within Different Conditions
Bodies Number Per 100 μm²
Total CHAF1A (or Mutant) Bodies
Total HP1α Bodies
Co-localized Bodies
siNC
siCHAF1A
CHAF1A-dHP1BD
CHAF1A-DS2-dHP1BD
O
SUV39H1 Bodies
within Different Conditions
Bodies Number Per 100 μm²
Total CHAF1A Bodies
Total SUV39H1 Bodies
Co-localized Bodies
siNC
siCHAF1A
P
SUV39H1 Bodies
within Different Conditions
% of Target Proteins within
Different Cellular Compartment
SUV39H1 within Nucleus
SUV39H1 within Cytoplasm
siNC
siCHAF1A
Q
SUV39H2 Bodies
within Different Conditions
Bodies Number Per 100 μm²
Total CHAF1A Bodies
Total SUV39H2 Bodies
Co-localized Bodies
siNC
siCHAF1A

Appendix Figure S7. Quantification analysis of cellular bodies upon CHAF1A knockdown.

A-J The line scan profiles of SIM images which showed co-localization and non-co-localization between two proteins.

K Quantification analysis of co-localization of two proteins. Percentages of target protein above threshold co-localized were calculated by measuring the percentages of co-localized target protein volume in total target protein volume.

L Pearson's coefficients in co-localized volume of each protein pairs were calculated based on the quantitation analysis results showed in (K). The co-localization value ranges between 1 and -1. A value of 1 represents perfect co-localization, 0 represents no co-localization, and -1 represents perfect inverse correlation.

M The percentages of cells with co-localized cellular bodies.

N The numbers of CHAF1A (or CHAF1A mutants) bodies, HP1α bodies and co-localized bodies per 100 μm^2 were measured in both siNC and siCHAF1A conditions.

O, P The numbers of CHAF1A bodies, SUV39H1 bodies and co-localized bodies per 100 μm^2 were measured in both siNC and siCHAF1A conditions (O). The percentages of SUV39H1 proteins within nucleus and cytoplasm were measured before and after CHAF1A knockdown (P).

Q The numbers of CHAF1A bodies, SUV39H2 bodies and co-localized bodies per 100 μm^2 were measured in both siNC and siCHAF1A conditions.

Data information: The scale bar of each SIM image represented 5 μm. All the samples were imaged to obtain at least three images. All the merged SIM images used for line scan profiling in (A-J) were from Fig 5A to Fig 5F.

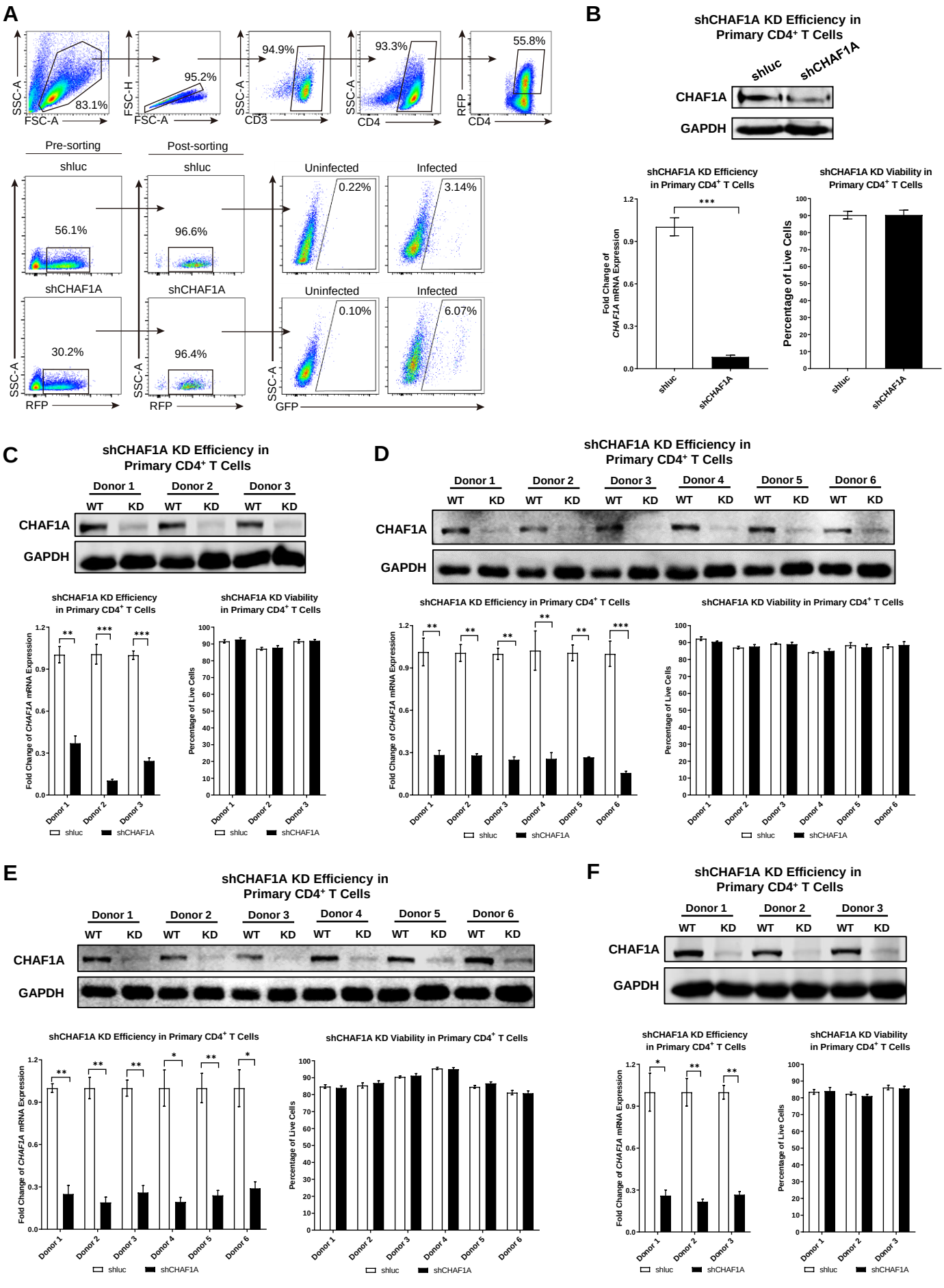
A
SSC-A
FSC-A
83.1%
FSC-H
95.2%
94.9%
CD3
93.3%
CD4
55.8%
RFP
Pre-sorting
Post-sorting
shluc
56.1%
96.6%
Uninfected
Infected
0.22%
3.14%
shCHAF1A
30.2%
96.4%
0.10%
6.07%
GFP
B
shCHAF1A KD Efficiency in Primary CD4+ T Cells
shluc
shCHAF1A
CHAF1A
GAPDH
shCHAF1A KD Efficiency in Primary CD4+ T Cells
Fold Change of CHAF1A mRNA Expression
***
shCHAF1A KD Viability in Primary CD4+ T Cells
Percentage of Live Cells
C
shCHAF1A KD Efficiency in Primary CD4+ T Cells
Donor 1
Donor 2
Donor 3
WT
KD
CHAF1A
GAPDH
shCHAF1A KD Efficiency in Primary CD4+ T Cells
Fold Change of CHAF1A mRNA Expression
shCHAF1A KD Viability in Primary CD4+ T Cells
Percentage of Live Cells
shluc
shCHAF1A
D
shCHAF1A KD Efficiency in Primary CD4+ T Cells
Donor 1
Donor 2
Donor 3
Donor 4
Donor 5
Donor 6
WT
KD
CHAF1A
GAPDH
shCHAF1A KD Efficiency in Primary CD4+ T Cells
Fold Change of CHAF1A mRNA Expression
shCHAF1A KD Viability in Primary CD4+ T Cells
Percentage of Live Cells
shluc
shCHAF1A
E
shCHAF1A KD Efficiency in Primary CD4+ T Cells
Donor 1
Donor 2
Donor 3
Donor 4
Donor 5
Donor 6
WT
KD
CHAF1A
GAPDH
shCHAF1A KD Efficiency in Primary CD4+ T Cells
Fold Change of CHAF1A mRNA Expression
shCHAF1A KD Viability in Primary CD4+ T Cells
Percentage of Live Cells
shluc
shCHAF1A
F
shCHAF1A KD Efficiency in Primary CD4+ T Cells
Donor 1
Donor 2
Donor 3
WT
KD
CHAF1A
GAPDH
shCHAF1A KD Efficiency in Primary CD4+ T Cells
Fold Change of CHAF1A mRNA Expression
shCHAF1A KD Viability in Primary CD4+ T Cells
Percentage of Live Cells
shluc
shCHAF1A

Appendix Figure S8. Knockdown efficiencies and corresponding viabilities in primary CD4$^+$ T cells.

A Gating strategies for HIV-1 latency models of primary CD4$^+$ T cells. Primary CD4$^+$ T cells were isolated through human CD4$^+$ T lymphocyte enrichment magnetic cell separation system (MACS). The purities of CD4$^+$ T cells were ensured at least 90%. Both CD3 and CD4 markers were used to sort RFP-positive CD4$^+$ T cells by fluorescence-activated cell sorting (FACS) system. RFP-positive CD4$^+$ T cells were shRNA lentiviruses-infected CD4$^+$ T cells. The purities of sorted shRNA lentiviruses-infected RFP-positive cells were ensured at least 90% by flow cytometry. The lentiviruses-infected CD4$^+$ T cells were infected with HIV-1 pseudotyped virus, or untreated (uninfected negative control). The uninfected negative controls were used to gate HIV-1 pseudotyped virus-infected GFP-positive cells.

B-F The efficiencies of shCHAF1A-mediated CHAF1A knockdown in primary CD4$^+$ T cells were confirmed by both WB and qPCR. The viabilities upon CHAF1A knockdown in each group were quantitated by measuring the percentages of amine-reactive fluorescent dye non-permeant cells.

Data information: Data represented mean ± SEM in triplicate. p-Values were calculated by Student's *t*-test. *p < 0.05, **p < 0.01, ***p < 0.001.

Source data are available online for this figure.